

A New Method of Modelling Tuneable Lasers with Functional Composition

B. Metherall

C. S. Bohun

November 13, 2019

Abstract

A new nonlinear model is proposed for tuneable lasers. Using the generalized nonlinear Schrödinger equation as a starting point, expressions for the transformations undergone by the pulse are derived for each of the five components (gain, loss, dispersion, modulation, and nonlinearity) within the laser cavity. These transformations are then composed to give the overall effect of one trip around the cavity.

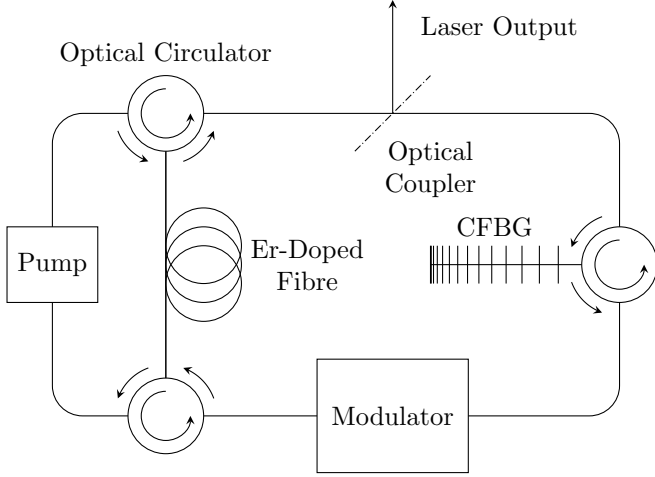


Figure 1: Typical cavity of a fibre based tuneable laser. The laser pulses travel clockwise around each loop.

1 Introduction

A tuneable laser has the ability to vary the frequency of its output by up to about 100 nanometres [1, 2, 3]. Tuneable lasers simultaneously lase at all frequencies within this bandwidth. This tuneability is quite useful and has applications in spectroscopy and high resolution imaging such as coherent anti-Stokes Raman spectroscopy and optical coherence tomography [1, 4, 3], as well as communications and diagnostics of ultra fast processes [5]. A typical tuneable laser cavity is shown in Figure 1. In contrast to a standard laser, a tuneable laser contains two additional components, namely, a chirped fibre Bragg grating (CFBG), and a modulator.

A CFBG is a length of optical fibre where the refractive index oscillates along its length [6], and therefore, can act as a reflective filter [7, 8, 6, 9]. Due to the oscillatory nature, light with the corresponding wavelength will be reflected when the Bragg condition is satisfied [7, 8, 10, 6, 5, 9]. The spacial variation of the refractive index effectively creates a spacial dependence on the Bragg condition, causing most wavelengths to be reflected by a CFBG, but with each wavelength satisfying the Bragg condition at a different spacial location¹. A consequence of this is that a time delay is created between wavelengths—this causes the pulse to disperse and broaden.

¹Note that a monotonic chirping ensures that the spacial dependence of the Bragg condition is continuous with respect to the frequency.

The modulator serves the purpose of reshaping the pulse. Without it, the pulse will repeatedly widen due to the CFBG—the modulator ensures the pulse is band limited by altering the envelope.

2 Modelling Efforts

The standard equation for studying nonlinear optics is the nonlinear Schrödinger equation (NLSE)²,

$$\frac{\partial A}{\partial z} = -i\frac{\beta_2}{2}\frac{\partial^2 A}{\partial T^2} + i\gamma|A|^2A. \quad (1)$$

Here $A = A(T, z) : \mathbb{R}^2 \mapsto \mathbb{C}$ is the complex pulse amplitude, $\beta_2 \in \mathbb{R}$ is the second order dispersion, and $\gamma \in \mathbb{R}$ is the coefficient of nonlinearity. In practice, (1) lacks a few key terms, thus, it is often generalized by adding amplification, loss, and occasionally higher order terms. This gives the generalized nonlinear Schrödinger equation (GNLSE) [11, 1, 12, 13, 14, 15],

$$\frac{\partial A}{\partial z} = -i\frac{\beta_2}{2}\frac{\partial^2 A}{\partial T^2} + i\gamma|A|^2A + \frac{1}{2}g(A)A - \alpha A, \quad (2)$$

where $g(A)$ is an amplifying term due to the gain, and $\alpha \in \mathbb{R}$ is the loss due to scattering and absorption.

The GNLSE has many applications in nonlinear optics and fibre optic communications, however, in the context of lasers we typically also add a modulation term. This yields the master equation of mode-locking [16, 17, 18, 19, 20, 21, 22, 23],

$$\frac{\partial A}{\partial z} = -i\frac{\beta_2}{2}\frac{\partial^2 A}{\partial T^2} + i\gamma|A|^2A + \frac{1}{2}g(A)A - \alpha A - M(T), \quad (3)$$

where $M(T)$ is the modulation function. The solutions of three simplifications of (3) have been investigated:

- Omitting both modulation and nonlinearity [16, 18, 19].
- Omitting only modulation [24, 23].
- Omitting only nonlinearity [4, 16, 17, 25, 20, 21, 22, 23].

For a more comprehensive history see [20].

²The NLSE can be derived from the nonlinear wave equation for electric fields; this derivation is presented in detail in [11, 6].

2.1 Discrete Models

While the derivation of (3) is correct mathematically, it is not representative of what happens within the laser cavity. The issue with (3) is that it has been assumed each process affects the pulse continuously within the cavity. As highlighted by Figure 1, this is a rather poor assumption. Within the cavity each effect is localized to its corresponding component: almost all of the dispersion happens within the CFBG [7], the pulse is only amplified within the Erbium-doped fibre, etc. Thus, perhaps a better model is one where (3) is broken down into the individual components giving the effect of each ‘block’ of the cavity. Each of the blocks can then be functionally composed together to give an iterative map for the effect of one circuit around the cavity. This transforms the differential equation into an algebraic equation.

Such a method was first proposed in 1955 by Cutler [26] while analyzing a microwave regenerative pulse generator. This method was adapted for mode-locked lasers in 1969 by Siegman and Kuizenga [27, 28]. Kuizenga and Siegman also had success experimentally validating their model [29, 30]. The effects of the nonlinearity would not be considered until Martinez, Fork, and Gordon [31, 32] tried modelling passively mode-locked lasers. This issue has recently been readdressed by Burgoyne [4] in the literature for tuneable lasers. In these models the effect of each block is described by a transfer function.

Despite the development of these block style models, several short-comings exist. The clearest is that none of these models have contained every block—either the nonlinearity or the modulation have been omitted. In the framework of tuneable lasers, each component plays a crucial role and the tuneable laser will not function correctly without the inclusion of all of the components. Another key drawback is that the functional operations of some of the components used in their models are phenomenological. While these functions are chosen based on the observed output, they are not necessarily consistent with the underlying physics. Finally, none of these previous models have been able to exhibit a phenomena called *wave-breaking* in which the self-phase modulation of the pulse becomes too strong, distorting and damaging the wave until it ultimately becomes unstable and unsustainable.

3 A New Model

Using the ideas presented in the previous section of the prior functional models [4, 26, 27, 29, 30, 31, 32, 28] we shall derive a new model from (2)—with the exception of the modulation in which we consider the exact functional form to be determined by the laser operator.

3.1 Components

We shall determine the effect each component has on the pulse by solving (2) while only considering the dominant term within each section of the cavity.

3.1.1 Gain

Within the Er-doped gain fibre, the gain term is dominant, and equation (2) reduces to

$$\frac{\partial A}{\partial z} = \frac{1}{2}g(A)A, \quad (4)$$

where $g(A)$ takes the form [1, 4, 16, 17, 19, 20, 24, 21, 13, 14, 5, 23, 15]

$$g(A) = \frac{g_0}{1 + E/E_{\text{sat}}}, \quad E = \int_{-\infty}^{\infty} |A|^2 dT, \quad (5)$$

where g_0 is a small signal gain, E is the energy of the pulse, and E_{sat} is the energy at which the gain begins to saturate. Without much difficulty this differential equation can be solved, and the effect on an incident pulse is

$$G(A; E) = \left(\frac{E_{\text{sat}}}{E} W \left(\frac{E}{E_{\text{sat}}} e^{E/E_{\text{sat}}} e^{g_0 L_g} \right) \right)^{1/2} A, \quad (6)$$

where L_g is the length of the gain fibre.

3.1.2 Nonlinearity

The nonlinearity of the fibre arises from the parameter γ ; in regions where this effect is dominant expression (2) becomes

$$\frac{\partial A}{\partial z} - i\gamma|A|^2 A = 0. \quad (7)$$

Using a similar method as with the gain, the effect of the nonlinearity can be shown to be

$$F(A) = A e^{i\gamma|A|^2 L_f}, \quad (8)$$

where L_f is the length of fibre.

3.1.3 Loss

Expression (2) leads to exponential decay due to the scattering and absorption of the fibre. However, a majority of the signal is removed from the cavity by the optical coupler. Combining these two effects yields

$$L(A) = (1 - R)e^{-\alpha L_T} A, \quad (9)$$

where R is the reflectivity of the output coupler, and L_T is the total length of the laser circuit as the effect of the losses³.

3.1.4 Dispersion

Considering only the dispersive terms of (2), one obtains

$$\frac{\partial A}{\partial z} = -i \frac{\beta_2}{2} \frac{\partial^2 A}{\partial T^2}. \quad (10)$$

The effect of dispersion is then given by the map

$$D(A) = \mathcal{F}^{-1} \left\{ e^{i\omega^2 L_D \beta_2 / 2} \mathcal{F}\{A\} \right\}, \quad (11)$$

where L_D is the length of the dispersive medium, and \mathcal{F} denotes the Fourier transform.

³Depending on the layout of the laser cavity the loss may take the form $L(A) = R e^{-\alpha L_T} A$ instead.

3.1.5 Modulation

In this model, the modulation is considered to be applied externally in which ever way the operator sees fit. For simplicity the representation is taken as the Gaussian

$$M(A) = e^{-T^2/2T_M^2} A, \quad (12)$$

where T_M is the characteristic width of the modulation.

3.2 Non-Dimensionalization

The structure of each process of the laser can be better understood by re-scaling the time, energy, and amplitude. Nominal values for tuneable lasers are shown in Table 1. Knowing experimental durations and energies, the table suggests the convenient scalings:

$$T = T_M \tilde{T}, \quad E = E_{\text{sat}} \tilde{E}, \quad A = \left(\frac{E_{\text{sat}}}{T_M} \right)^{1/2} \tilde{A}. \quad (13)$$

Revisiting each process map shows each process has a characteristic non-dimensional parameter. The new mappings—after dropping the tildes—are

$$\begin{aligned} G(A) &= (E^{-1} W(aEe^E))^{1/2} A, & F(A) &= Ae^{ib|A|^2} \\ D(A) &= \mathcal{F}^{-1} \left\{ e^{is^2\omega^2} \mathcal{F}\{A\} \right\}, & L(A) &= hA, \\ M(A) &= e^{-T^2/2} A, \end{aligned} \quad (14)$$

with the four dimensionless parameters, as defined by the values in Table 1,

$$\begin{aligned} a &= e^{g_0 L_g} \sim 8 \times 10^3, & h &= (1-R)e^{-\alpha L} \sim 0.04, \\ b &= \gamma L_f \frac{E_{\text{sat}}}{T_M} \sim 1, & s &= \sqrt{\frac{\beta_2 L_D}{2T_M^2}} \sim 0.2, \end{aligned} \quad (15)$$

which characterize the behaviour of the laser. Notice that the modulation is only characterized by T_M , and each other process has its own independent non-dimensional parameter.

3.3 Combining the Effects of Each Block of the Model

In this model the pulse is iteratively passed through each process, the order of which must now be considered. We are most interested in the output of the laser cavity, and so we shall start with the loss component. Next the pulse is passed through the CFBG, as well as the modulator. Finally, the pulse travels through the gain fibre to be amplified, and then we consider the effect of the nonlinearity since this is the region where the power is maximal. Note that in general the functional operators of the components do not commute, and therefore the order of the components is indeed important—in contrast to the previous models. This is especially the case of dispersion as realized through the Fourier transform. Functionally this can be denoted as

$$\mathcal{L}(A) = F(G(M(D(L(A))))) , \quad (16)$$

where \mathcal{L} denotes one loop of the laser. The pulse after one complete circuit of the laser cavity is then passed back in to restart the process. A steady solution to this model is one in which the envelope and chirp are unchanged after traversing every component in the cavity—we are uninterested in the phase. That is, such that $\mathcal{L}(A) = Ae^{i\phi}$ —for some $\phi \in \mathbb{R}$.

4

In the case $b = 0$ a solution can be found analytically. We would expect the solution will have the form of a Gaussian. There are a few reasons for this; the solution to previous models were Gaussian [26, 28, 27, 31, 32], the equilibrium shape will be highly correlated to the shape of the modulation function, and since a Gaussian is a fixed point of the Fourier transform [38] dispersion will not alter the envelope.

To compute $\mathcal{L}(A)$, consider the pulse

$$A = \sqrt{P} \exp \left(-(1+iC) \frac{T^2}{2\sigma^2} \right) e^{i\phi_0}, \quad (17)$$

where P is the peak power, C is the chirp, σ^2 is the variance, and ϕ_0 is the initial phase. This form is chosen because it resembles the envelope and linear chirping found by experiment ***cite. Having neglected the effect of the nonlinearity $\mathcal{L}(A)$ can be found analytically from the process mappings (14). By assuming the pulse in (17) is in equilibrium, we find that the variance must satisfy

$$\sigma^8 + 4s^4\sigma^6 - 20s^4\sigma^4 + 32s^4\sigma^2 - 16s^4 = 0. \quad (18)$$

As this expression is a quartic in σ^2 it too has an analytic solution, namely,

$$\sigma^2 = \sqrt{2}s \left(s^6 + 3s^2 + \sqrt{4+s^4}(1+s^4) \right)^{1/2} - s^4 - s^2 \sqrt{4+s^4}. \quad (19)$$

However, by asymptotically expanding (18) we find the useful relations

$$\sigma^2 \sim \begin{cases} 2s(1-s) + \mathcal{O}(s^3) & s \rightarrow 0 \\ 1 - \frac{1}{4}s^{-4} + \frac{3}{8}s^{-8} + \mathcal{O}(s^{-12}) & s \rightarrow \infty \end{cases}. \quad (20)$$

Additionally, from the variance we can determine the behaviour of the chirp to be

$$C \sim \begin{cases} 1-s + \frac{1}{2}s^2 + \mathcal{O}(s^3) & s \rightarrow 0 \\ \frac{1}{2}s^{-2} - \frac{3}{8}s^{-6} + \mathcal{O}(s^{-10}) & s \rightarrow \infty \end{cases}. \quad (21)$$

$$E = \frac{h^2 \zeta^2}{1 - h^2 \zeta^2} \log(ah^2 \zeta^2). \quad (22)$$

$$(23)$$

$$P = \frac{W(aEe^E)}{\sqrt{\pi}\sigma}. \quad (24)$$

5

We shall now consider the nonlinear case—when $b > 0$. In this case it becomes impossible to obtain an analytic result. Recall from (??) that the nonlinearity takes the form

$$F(A) = Ae^{ib|A|^2}.$$

This is a highly nonlinear operator, and attempting to compute the Fourier transform analytically of a pulse that has undergone the transformation due to the nonlinearity is futile. Instead we must resort to a numerical solution.

Parameter	Symbol	Value	Sources
Absorption of Fibre	α	10^{-4} – 0.3 m^{-1}	[33, 14, 34, 23, 15]
Fibre Dispersion	β_2^f	-50 – $50 \text{ ps}^2/\text{km}$	[7, 11, 4, 35, 13, 15]
Fibre Nonlinearity	γ	0.001 – $0.01 \text{ W}^{-1}\text{m}^{-1}$	[11, 12, 23, 15]
Grating Dispersion	$\beta_2^g L_D$	10 – 2000 ps^2	[7, 11, 4, 36]
Length of Cavity	L_T	10 – 100 m	[33, 13, 22]
Length of Fibre	L_f	0.15 – 1 m	[33]
Length of Gain Fibre	L_g	2 – 3 m	[4, 13, 14, 37, 15]
Modulation Time	T_M	15 – 150 ps	[1, 33, 4]
Reflectivity of Optical Coupler	R	0.1 – 0.9	[33, 36, 13, 37, 22, 3]
Saturation Energy	E_{sat}	10^3 – 10^4 pJ	[33, 23, 15]
Small Signal Gain	g_0	1 – 10 m^{-1}	[33, 15]

Table 1: Range of variation of various parameters.

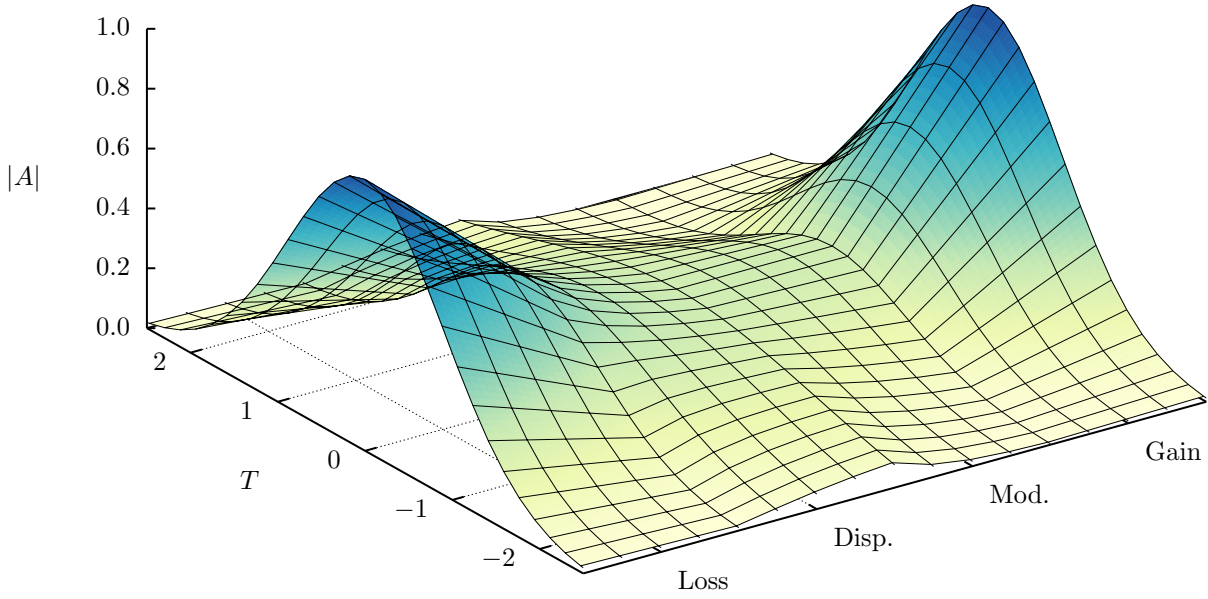


Figure 2:

With the inclusion of the nonlinearity we generally find a similar solution to the linear case. An example of this is shown in Figure ?? . The envelope of the pulse is unsurprisingly Gaussian-esque, however, it is *not* precisely Gaussian and more closely resembles a generalized Gaussian⁴. The fact that the pulse envelope is not Gaussian is further emphasized while examining the Fourier transform of the pulse. If the pulse were a Gaussian, we would expect the Fourier transform to also be a Gaussian [39, 38]. Instead, the magnitude of the Fourier transform has a unique weakly bi-modal shape. This deviation suggests the nonlinearity implants higher frequency oscillations into the pulse—a key observation in the coming subsections. Finally, we shall examine the derivative of the phase—essentially the chirp. Recall in Chapter ?? the chirp was defined as coefficient of $-\frac{1}{2}iT^2$ in the exponential, and by taking the negative of the derivative we would expect a linear function with a slope equal to the chirp. In the nonlinear case, we recover this linear response for moderate values of T . However, for $|T| > 1$ the chirp begins to saturate. This is consistent with the experimental results [40, 41, 34].

The noise in the energy exhibited for moderate to large values of b , and small values of s is a phenomenon called *wave breaking* [11, 42, 12, 41, 34]. Wave breaking is not limited to just optics; wave breaking occurs in areas such as plasmas, transmission lines, and fluid dynamics [41]. Wave breaking occurs because the pulse begins to interfere with itself in a way called SPM [7, 11, 10]. SPM occurs because the index of refraction is intensity dependent [7, 10, 41, 5], which leads to additional chirp across the pulse [11, 42, 41, 5]. This in turn causes higher order frequencies to be injected into the pulse [11, 42], as we saw in Figure ?? . These high frequencies compound with each trip around the cavity becoming parasitic very quickly—Figure ?? highlights this. Notice that the difference between Figure ?? and Figure ?? is a difference in b of 0.05—just enough to cross the boundary—this difference could be attributed to adding a few centimetres more of fibre between the gain and output coupler.

The left figures show the pulse after 11 trips around the cavity; in the Fourier transform it is clear that the contributions from higher frequencies has increased. We obtain comparable results as in the experiments [42, 41]. Additionally, the chirp starts losing its linearity causing it to start becoming unstable; the nature of this instability is again in agreement with the experiments [42, 41]. The parasitic nature of the high frequency contributions is evident by examining the right figures. After five additional trips around the cavity, the envelope of the pulse is much more rippled, and the real and imaginary parts become incoherent. Moreover, the Fourier transform has no clear structure and has essentially become noise. The chirp has grown to be highly oscillatory and unstable. Once the pulse has reached a state such as this, the envelope, Fourier transform, and chirp never reach a steady equilibrium state.

To obtain a better understanding of how the pulse either converges to equilibrium, or diverges to wave breaking, we shall examine the difference between the envelopes of consecutive iterations. More precisely, we compute the error

by

$$E = \frac{\| |A_i| - |A_{i-1}| \|_2}{\| A_{i-1} \|_2}, \quad (25)$$

where $\| \cdot \|_2$ denotes the $L^2(\mathbb{R})$ norm, which is computed numerically using the trapezoid rule ($N = 2^{12}$). Notice as well that in the numerator we use the modulus of the pulses, again this is because we are uninterested in the phase shift between iterations. A plot of the error can be found in Figure ?? , with $i = 100$. The standard method would be to iterate until a fixed tolerance is reached, however, there are some reasons that make a fixed number of iterations preferable—as long as a sufficient number is chosen. The main reason is that this allows us to observe a richer structure than simply whether or not the tolerance had been reached by some maximum number of iterations. Additionally, incorrectly choosing the critical tolerance could easily lead to erroneous categorizations at points. As we saw in Figure ?? some values of the parameters lead to a steady, periodic state, but with an error of $\mathcal{O}(10^{-6})$, and so, had we set the tolerance to 10^{-8} these points would have been labeled as unsteady.

Unsurprisingly, the error is largest in the region where the wave breaks. As mentioned in the previous subsection, the pulse does not reach a stable state in this region. As a consequence the envelope varies drastically, which leads to this large error. Conversely, the region where the energy appeared to be stable still has a non-zero error. The cause of this discrepancy is because some equilibrium states have a periodicity greater than 1, thus, we redefine (25) to be instead

$$E_\Delta = \frac{\| |A_i| - |A_{i-\Delta}| \|_2}{\| A_{i-\Delta} \|_2}, \quad (26)$$

to pick up equilibrium states with period Δ , again with $i = 100$. Figure ?? shows the error for an assortment of Δ values. There are several key observations to make, first, for $\Delta = 2$ the kidney-shaped blob in the lower right corner has vanished, thus, this entire region has a periodicity of 2. Second, for $\Delta = 3$ in the upper right corner a negative triangular-shaped structure emerges. Lastly, $\Delta \in \{5, 7, 11, 13\}$ may not seem to extract any higher order periods, however, there are in fact very small striations in the lower left. We typically chose Δ values to be prime since they are the building blocks for composite numbers. However, there are two composite Δ values of interest. The first is 16, since $16 = 2^4$, as it will pick up any periodic behaviour with orders of 2, 4, 8, 16. Lastly, we chose $\Delta = 60$ for a similar reason: because 60 is highly divisible we can extract orders such as 12 or 30 without having to explicitly run the calculations⁵.

The last item we wish to consider is the order in which the components are placed. In Section 3.3 a brief description for the choice of the order was given. We start with the loss component since this coincides with the output; the fibre nonlinearity follows the gain since this is where it has the largest impact; and the loss follows the nonlinearity in an attempt to mitigate its effect. Therefore, the loss is first, and the gain followed by the nonlinearity are last—leaving

⁴A generalized Gaussian has the form $\exp(-t^\alpha)$, with $\alpha > 2$.

⁵In the case of $\Delta = 60$ a value of $i = 150$ is used to ensure sufficient iterations to converge.

dispersion and modulation in the middle. We chose to put the dispersion block ahead of the modulator. However, there was no real reason behind this—modulation before dispersion is equally as valid—and in this subsection we explore the effect of modulating the pulse before it passes through the CFBG.

The result of this switch is shown in Figure ?? . As a whole, unsurprisingly, we find the same behaviour and structure, however, there are some intriguing differences. Perhaps the most interesting is the small island of instability in Figure ?? at around $s = 0.075$, $b = 1.1$ which was not present in the other ordering. Within this island the wave is unstable and breaks, but, curiously there is a small gap between this island and the main unstable region. We find more distinctions when considering the larger area in Figure ?? . Again, the structure and periodic nature of the boundary is similar to before, however, this boundary has shifted rightwards to a larger s value. Additionally, within the unstable region the density of the contour lines is much greater—suggesting it is in some sense more chaotic and random than with the components in their original permutation. The final main difference between the two orderings, is that in this case the energy contours are no longer monotonic functions of s . Instead we find a parabolic shape on the top contour, and two lobes on the second contour.

6 Conclusion

Within this paper we developed a new nonlinear model for tuneable lasers. In order to better represent the underlying physics within the laser cavity the nonlinear Schrödinger equation was reduced to simpler differential equations for each component of the laser. This led to a functional map that defines the effect of each component on a particular input pulse. These processes were then composed together to give an iterative mapping of the whole laser cavity. In a future publication we shall show the results obtained by this iterative mapping as well as discuss the dynamics exhibited by this model—including wave-breaking—to predict the conditions under which the pulse is stable and sustainable.

References

- [1] C. S. Bohun, Y. Cher, L. J. Cummings, P. Howell, T. Mitre, L. Monasse, J. Mueller, and S. Rouillon, “Modelling and Specifying Dispersive Laser Cavities,” in *Sixth Montréal Industrial Problem Solving Workshop*, pp. 11–25, 2015.
- [2] B. Burgoyne and A. Villeneuve, “Programmable Lasers: Design and Applications,” in *Proc.SPIE*, vol. 7580, 2010.
- [3] S. Yamashita, Y. Nakazaki, R. Konishi, and O. Kusakari, “Wide and Fast Wavelength-Swept Fiber Laser Based on Dispersion Tuning for Dynamic Sensing,” *Journal of Sensors*, vol. 2009, 2009.
- [4] B. Burgoyne, A. Dupuis, and A. Villeneuve, “An Experimentally Validated Discrete Model for Dispersion-Tuned Actively Mode-Locked Lasers,” *IEEE Journal of Selected Topics in Quantum Electronics*, vol. 20, pp. 390–398, Sept 2014.
- [5] W. T. Silfvast, *Laser Fundamentals*. Cambridge University Press, 2 ed., 2004.
- [6] M. F. S. Ferreira, *Nonlinear Effects in Optical Fibers*. John Wiley & Sons, Inc., 2011.
- [7] G. Agrawal, *Fiber-Optic Communication Systems*. John Wiley & Sons, Inc., 3 ed., 2002.
- [8] A. Al-Azzawi, *Fiber Optics: Principles and Advanced Practices*. CRC Press, 2 ed., 2017.
- [9] A. N. Starodoumov, “Optical Fibers and Accessories,” in *Advanced Optical Instruments and Techniques* (D. Malacara-Hernández and B. J. Thompson, eds.), vol. 2 of *Handbook of Optical Engineering*, pp. 633–676, CRC Press, 2 ed., 2018. Ch. 18. 2018.
- [10] P. C. Becker, N. A. Olsson, and J. R. Simpson, *Erbium-Doped Fiber Amplifiers Fundamentals and Technology*. Academic Press, 1 ed., 1999.
- [11] G. Agrawal, *Nonlinear Fiber Optics*. Academic Press, 5 ed., 2013.
- [12] C. Finot, B. Kibler, L. Provost, and S. Wabnitz, “Beneficial Impact of Wave-Breaking for Coherent Continuum Formation in Normally Dispersive Nonlinear Fibers,” *J. Opt. Soc. Am. B*, vol. 25, pp. 1938–1948, Nov 2008.
- [13] J. Peng, H. Luo, and L. Zhan, “In-Cavity Soliton Self-Frequency Shift Ultrafast Fiber Lasers,” *Opt. Lett.*, vol. 43, pp. 5913–5916, Dec 2018.
- [14] O. V. Shtyrina, A. V. Ivanenko, I. A. Yarutkina, A. V. Kemmer, A. S. Skidin, S. M. Kobtsev, and M. P. Fedoruk, “Experimental Measurement and Analytical Estimation of the Signal Gain in an Er-Doped Fiber,” *J. Opt. Soc. Am. B*, vol. 34, pp. 227–231, Feb 2017.
- [15] I. Yarutkina, O. Shtyrina, M. Fedoruk, and S. Turitsyn, “Numerical Modeling of Fiber Lasers with Long and Ultra-long Ring Cavity,” *Opt. Express*, vol. 21, pp. 12942–12950, May 2013.
- [16] H. A. Haus, “A Theory of Forced Mode Locking,” *IEEE Journal of Quantum Electronics*, vol. 11, pp. 323–330, July 1975.
- [17] H. A. Haus, *Waves and Fields in Optoelectronics*. Prentice-Hall, Inc., 1984.
- [18] H. A. Haus, “Laser Mode Locking with Addition of Nonlinear Index,” *IEEE Journal of Quantum Electronics*, vol. 22, pp. 325–331, Feb 1986.
- [19] H. A. Haus, “Analytic Theory of Additive Pulse and Kerr Lens Mode Locking,” *IEEE Journal of Quantum Electronics*, vol. 28, pp. 2086–2096, Oct 1992.
- [20] H. A. Haus, “Mode-Locking of Lasers,” *IEEE Journal of Selected Topics in Quantum Electronics*, vol. 6, pp. 1173–1185, Nov 2000.
- [21] F. Kärtner, “Lecture Notes in Ultrafast Optics.” Online, Spring 2005. Massachusetts Institute of Technology: MIT OpenCourseWare.

- [22] K. Tamura and M. Nakazawa, "Dispersion-Tuned Harmonically Mode-Locked Fiber Ring Laser for Self-Synchronization to an External Clock," *Opt. Lett.*, vol. 21, pp. 1984–1986, Dec 1996.
- [23] N. G. Usechak and G. P. Agrawal, "Rate-Equation Approach for Frequency-Modulation Mode Locking using the Moment Method," *J. Opt. Soc. Am. B*, vol. 22, pp. 2570–2580, Dec 2005.
- [24] H. A. Haus, J. G. Fujimoto, and E. P. Ippen, "Structures for Additive Pulse Mode Locking," *J. Opt. Soc. Am. B*, vol. 8, pp. 2068–2076, Oct 1991.
- [25] H. A. Haus, "Theory of Soliton Stability in Asynchronous Modelocking," *Journal of Lightwave Technology*, vol. 14, pp. 622–627, April 1996.
- [26] C. C. Cutler, "The Regenerative Pulse Generator," in *Proceedings of the IRE*, IEEE, Feb 1955.
- [27] D. J. Kuizenga and A. E. Siegman, "FM and AM Mode Locking of the Homogeneous Laser - Part I: Theory," *IEEE Journal of Quantum Electronics*, vol. 6, pp. 694–708, Nov 1970.
- [28] A. E. Siegman and D. J. Kuizenga, "Simple Analytic Expressions for AM and FM Modelocked Pulses in Homogenous Lasers," *Appl. Phys. Lett.*, pp. 181–182, Mar 1969.
- [29] D. J. Kuizenga and A. E. Siegman, "FM and AM Mode Locking of the Homogeneous Laser - Part II: Experimental Results in a Nd:YAG Laser with Internal FM Modulation," *IEEE Journal of Quantum Electronics*, vol. 6, pp. 709–715, Nov 1970.
- [30] D. J. Kuizenga and A. E. Siegman, "FM-Laser Operation of the Nd:YAG Laser," *IEEE Journal of Quantum Electronics*, vol. 6, pp. 673–677, Nov 1970.
- [31] O. E. Martinez, R. L. Fork, and J. P. Gordon, "Theory of Passively Mode-Locked Lasers Including Self-Phase Modulation and Group-Velocity Dispersion," *Opt. Lett.*, vol. 9, pp. 156–158, May 1984.
- [32] O. E. Martinez, R. L. Fork, and J. P. Gordon, "Theory of Passively Mode-Locked Lasers for the Case of a Nonlinear Complex-Propagation Coefficient," *J. Opt. Soc. Am. B*, vol. 2, pp. 753–760, May 1985.
- [33] B. Burgoyne. Private Communication, 2018.
- [34] W. J. Tomlinson, R. H. Stolen, and A. M. Johnson, "Optical Wave Breaking of Pulses in Nonlinear Optical Fibers," *Opt. Lett.*, vol. 10, pp. 457–459, Sept 1985.
- [35] N. M. Litchinitser, B. J. Eggleton, and D. B. Patterson, "Fiber Bragg Gratings for Dispersion Compensation in Transmission: Theoretical Model and Design Criteria for Nearly Ideal Pulse Recompression," *Journal of Lightwave Technology*, vol. 15, pp. 1303–1313, Aug 1997.
- [36] S. Li and K. T. Chan, "Electrical Wavelength Tunable and Multiwavelength Actively Mode-Locked Fiber Ring Laser," *Applied Physics Letters*, vol. 72, no. 16, pp. 1954–1956, 1998.
- [37] K. Tamura, E. P. Ippen, H. A. Haus, and L. E. Nelson, "77-fs Pulse Generation from a Stretched-Pulse Mode-Locked All-Fiber Ring Laser," *Opt. Lett.*, vol. 18, pp. 1080–1082, Jul 1993.
- [38] I. S. Gradshteyn and I. M. Ryzhik, *Table of Integrals, Series, and Products*. Academic Press, 7 ed., 2007.
- [39] L. Debnath and D. Bhatta, *Integral Transforms and Their Applications*. Chapman & Hall/CRC Press, 2 ed., 2007.
- [40] Q. Chen, N. Lu, and F. Jiang, "Characterization of the Dispersion of Chirped Fiber Bragg Grating Through Fourier Transform Spectrometry Method," in *Proc.SPIE*, vol. 6837, 2008.
- [41] J. E. Rothenberg, "Femtosecond Optical Shocks and Wave Breaking in Fiber Propagation," *J. Opt. Soc. Am. B*, vol. 6, pp. 2392–2401, Dec 1989.
- [42] D. Anderson, M. Desaix, M. Lisak, and M. L. Quiroga-Teixeiro, "Wave Breaking in Nonlinear-Optical Fibers," *J. Opt. Soc. Am. B*, vol. 9, pp. 1358–1361, Aug 1992.